Earth and Planetary Science Letters 513 (2019) 187–196

Contents lists available at ScienceDirect

Earth and Planetary Science Letters

www.elsevier.com/locate/epsl

Geochemical evidence for expansion of marine euxinia during an early Silurian (Llandovery–Wenlock boundary) mass extinction

Seth A. Young *, Andrew Kleinberg, Jeremy D. Owens

Department of Earth, Ocean and Atmospheric Science and National High Magnetic Field Laboratory, Florida State University, Tallahassee, FL 32306, United States of America

ARTICLE INFO

Article history:
Received 6 September 2018
Received in revised form 13 February 2019
Accepted 17 February 2019
Available online xxxx
Editor: D. Vance

Keywords:
Ireviken extinction event
sulfur isotope
iodine
anoxia
euxinia
modeling

ABSTRACT

Repeated biotic crises have become the hallmark for the Silurian with the three most significant marine turnover events being related to dramatic global environmental perturbations. Causal mechanisms linking these marine extinction events with positive carbon isotope ($\delta^{13}C$) excursions, paleoceanographic change, and climate remain poorly constrained. Here, we examine the positive $\delta^{13}C$ excursion across the Llandovery/Wenlock boundary, and the associated Ireviken extinction event. This positive $\delta^{13}C$ excursion has been interpreted to reflect a major change in global oceanographic-climate state and enhanced organic carbon burial. New geochemical data from two paleocean basins have been analyzed to determine local and global redox conditions using carbon- and sulfur-isotopes ($\delta^{34}S$), and iodine (I/Ca+Mg) proxies. The high-resolution $\delta^{13}C$ and $\delta^{34}S$ data from both sections show positive excursions indicative of global perturbations to each of these elemental cycles, with minimal temporal offsets between the two systems. Numerical box modeling of $\delta^{13}C$ and $\delta^{34}S$ data indicates that these isotopic shifts can be generated by significant increases in the burial of organic carbon and pyrite, which are most likely due to enhanced burial under euxinic (anoxic and sulfidic) conditions. Independently, I/(Ca+Mg) values point to locally anoxic bottom waters in the distal and deeper basinal setting in Nevada before, during, and after the Ireviken positive $\delta^{13}C$ excursion. I/(Ca+Mg) values in the proximal shelf setting in Tennessee show relatively oxic waters during the onset of peak $\delta^{13}C$ values, after which bottom-water oxygen concentrations dropped throughout the remainder of the excursion. This multiproxy paleoredox dataset provides the first direct evidence for local and global expansion of reducing marine conditions coincident with the Silurian biotic event and positive $\delta^{13}C$ excursion. Integration of these geochemical data for local- and global-scale changes in marine redox conditions with the paleontological data and evidence for eustatic sea-level rise points toward a shoaling of anoxic and/or euxinic waters onto the shelf as a driver for the Ireviken extinction event.

1. Introduction

The Silurian Period was one of the most intense intervals of environmental and biological change in the Paleozoic (Munnecke et al., 2003; Saltzman, 2005; Cramer et al., 2010; Cooper et al., 2014; Trotter et al., 2016). This period is characterized by recurrent environmental/oceanographic changes that have been linked to numerous marine extinctions, many of which are associated with perturbations in the global carbon cycle (e.g., Jeppsson, 1998; Munnecke et al., 2003, 2010; Cramer and Saltzman, 2005; Calner, 2008). There are at least three major Silurian positive carbon isotope excursions (CIEs; $\geq +4‰$) that coincide with major biotic events, however, the exact cause(s) of these events remain poorly understood. Specifically, the links between marine redox state, atmospheric pO_2 and pCO_2 levels, and global weathering rates (biogeochemical nutrient cycling/delivery) are all poorly constrained in the Paleozoic (e.g., Berner et al., 2007; Gill et al., 2007; Edwards et al., 2017). Paleoceanographic models for these Silurian events make broad-scale inferences about marine redox conditions based upon the cyclic lithologies, conodont distributions, and stable carbon ($\delta^{13}C$) and oxygen ($\delta^{18}O$) isotope trends observed within epeiric seas (Bickert et al., 1997; Jeppsson, 1998; Cramer and Saltzman, 2007).

Traditionally studies documenting parallel $\delta^{13}C$ and sulfur ($\delta^{34}S_{CAS}$; carbonate-associated sulfate) excursions are interpreted to indicate changes in global marine redox conditions (expansion of anoxic and/or sulfidic conditions) that lead to higher burial rates

* Corresponding author.
E-mail address: sayoung2@fsu.edu (S.A. Young).

https://doi.org/10.1016/j.epsl.2019.02.023
0012-821X/

of organic matter and pyrite (Gill et al., 2007, 2011; Owens et al., 2013; Young et al., 2016; Edwards et al., 2018). These well-established isotope systems can provide first-order approximations of the global extent of anoxia, or more specifically euxinia (anoxic and sulfidic water-column). However, these model estimates utilize modern observations and parameters, and therefore require assumptions about the homogeneity, reservoir sizes, and fluxes of global marine sulfate and DIC (dissolved inorganic carbon) pools (Kump and Arthur, 1999; Kurtz et al., 2003). While models of the paired carbon and sulfur systems provide valuable information about the dynamics of marine redox conditions on a global scale, they do not resolve local or basinal redox dynamics. Recently, I/Ca values have been developed as a local redox proxy in carbonate depositional environments (Lu et al., 2010, 2018; Hardisty et al., 2014). When used individually these geochemical proxies are limited in the spatiotemporal resolution of the marine redox conditions. However, when combined with several independent geochemical proxies, a broader local to global picture can be attained (Owens et al., 2017).

The most severe of the Silurian marine extinction events have been recognized globally (including the late Llandovery–early Wenlock Ireviken Event), and they have strikingly similar anachronistic sedimentary facies and faunal changes to the "big five" Phanerozoic mass extinctions (e.g., Calner, 2008). The Llandovery–Wenlock boundary interval is well-studied, with paleontological data documenting a stepwise extinction interval known as the Ireviken Event (e.g., Jeppsson, 1997, 1998), *Cyrtograptus murchisoni* Event in graptolite taxa (Melchin et al., 1998), and an associated Ireviken positive CIE (Saltzman, 2001; Munnecke et al., 2003; Cramer and Saltzman, 2005, 2007). Furthermore, these studies provide the basis for the proposed Silurian ocean-climate models (e.g., Jeppsson, 1998). An integrated multi-proxy geochemical approach provides an opportunity to directly test the stratigraphic extent and magnitude of local to global redox perturbations associated with the known CIE and associated extinction. In this study, we investigated two early Silurian (Telychian–Sheinwoodian stages) carbonate successions, one in the Great Basin and another in the Midcontinent regions of North America (Fig. 1) where previous biostratigraphic (Klapper and Murphy, 1975; Berry and Murphy, 1975; Barrick, 1983) and $\delta^{13}C$ studies (e.g., Cramer and Saltzman, 2005; Saltzman, 2001) have documented the event. We present new $\delta^{34}S_{CAS}$ data and sedimentary pyrite ($\delta^{34}S_{pyr}$), I/Ca, $\delta^{13}C_{carb}$ (carbonates), and $\delta^{13}C_{org}$ (organic matter) measurements. This is the first study to combine geochemical datasets to constrain local to global redox conditions, geochemical box model simulations, along with previously published sea-level reconstructions, to better constrain the potential mechanism(s) driving the known extinction record.

2. Background

2.1. Geologic setting Nevada and Tennessee

The Pete Hanson Creek II section is located in the northern portion of the Roberts Mountains of central Nevada. This section is interpreted as an upper continental slope setting below the shelf-slope break (Johnson and Murphy, 1984), and was located on the western margin of Laurentia in the Panthalassic Ocean (Fig. 1). A thick interval of bedded black chert marks the base of the section (Fig. 2) and likely represents an upwelling region to the west of the Laurentian margin (e.g., Cramer and Saltzman, 2007). Previous biostratigraphic work constrains the chert-rich lower part of the Roberts Mountains Formation within the *Pterospathodus celloni* conodont biozone and *Monoclimacis crenulata–Oktavites spiralis* graptolite biozones of the Telychian Stage, and then transitions to carbonate mudstone–wackestone facies within the *Pterospathodus*

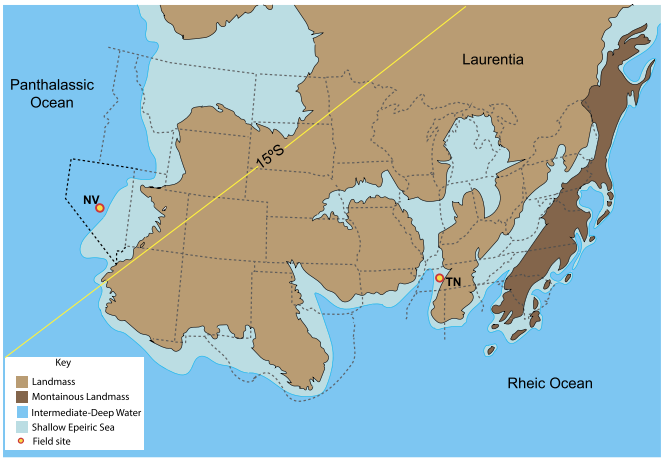

Fig. 1. Paleogeographic reconstruction of Laurentia during the early Silurian (435 Myr ago) with approximate locations of the Nevada (NV) and Tennessee (TN) study sites (red-yellow circles). (For interpretation of the colors in the figure(s), the reader is referred to the web version of this article.)

amorphognathoides biozone (Klapper and Murphy, 1975). Though the upper portion of this section lacks conodont biostratigraphic control, middle-late Sheinwoodian Stage graptolites, *C. rigidus* and *C. perneri*, have been documented in this part of the section (Berry and Murphy, 1975). These previous biostratigraphic investigations constrain a $\delta^{13}C_{carb}$ study that documents the complete Ireviken CIE record at this site (Saltzman, 2001).

The Newsom Roadcut field locality is west of Nashville, TN, (north of I-40 along McCrory Lane) and is interpreted to have been deposited in a shallow inner- to mid-rimmed-shelf environment (Barrick, 1983 and references within) with a direct connection to the Rheic Ocean. Conodont biostratigraphy reported from the Wayne Formation (Maddox Member) has constrained the timeframe of its deposition spanning the latest Llandovery to early Wenlock (Barrick, 1983). The basal beds of the formation correlate with the *P. amorphognathoides* conodont biozone, which has been identified globally at or near the base of the Ireviken CIE (Saltzman, 2001; Cramer and Saltzman, 2005, 2007; Cramer et al., 2010). This section experienced longer erosional/non-depositional effects during the late Llandovery eustatic sea-level lowstand, and therefore the basal Wayne Formation does not record pre-excursion baseline $\delta^{13}C_{carb}$ values nor part of the rising limb of the Ireviken CIE (Fig. 3). The base of the Maddox Member consists of a calcareous ferruginous siltstone unit, interpreted to represent the onset of eustatic sea-level rise, that transitions into an argillaceous packstone at ~1.2 m. Additional diagnostic conodonts, *Ozarkodina sagitta rhenana*, and *Kockelella walliseri*, have been recovered from this section (Barrick, 1983) at the 3.0 to 3.2 m interval, which allows for precise correlation to other carbonate sections of mid-Sheinwoodian age, the *O. s. rhenana* Zone (McAdams et al., 2019). Continued early Wenlock sea-level rise is indicated by the shift in lithology to a skeletal packstone–wackestone, eventually reaching maximum highstand as interpreted from the change to skeletal wackestone at ~6 m. Above this interval, the transition back to interbedded skeletal packstone–wackestone represents an overall eustatic sea-level fall (Cramer and Saltzman, 2005).

2.2. $\delta^{13}C_{carb}$ and $\delta^{34}S_{CAS}$ as global proxies

Sulfur is removed from the oceans by the deposition of sulfate evaporite deposits, carbonate-associated sulfate, and burial of microbially mediated sedimentary pyrite. Microbial sulfate reducers produce hydrogen sulfide (H_2S) as a waste product as part of their metabolism and, in the presence of reactive Fe, sulfide minerals

like pyrite (FeS_2) are rapidly (hours to 10s–100s of years, depending upon Fe-bearing minerals present) precipitated (e.g., Canfield et al., 1992). In modern ocean settings microbial sulfate reduction (MSR) primarily occurs in the sediments, but when it occurs in the water column biological stress is often observed because H_2S is toxic to most aerobic organisms (Vaquer-Sunyer and Duarte, 2010 and references therein). MSR-produced H_2S is isotopically depleted in ^{34}S by nearly 70‰ in natural environments such as the Black Sea (Fry et al., 1991). Coupled carbon and sulfur isotopic analyses provide the possibility to document past fluctuations in the carbon and sulfur cycles, and in turn provide unique insights into ocean-atmosphere redox evolution (Adams et al., 2010; Gill et al., 2011; Owens et al., 2013; Sim et al., 2015). Due to the fact that residence times of carbon (10^5 yr) and sulfate (10^6 yr) in the global oceans are significantly longer than interocean mixing (10^3 yr) they are considered homogeneous and their stable isotopic compositions representative of global seawater. However, we recognize that there are processes that can decouple $\delta^{13}C_{carb}$ values from the global DIC reservoir, and that can lead to lateral gradients in $\delta^{13}C$, up to 2‰ in restricted carbonate settings compared to the open ocean (e.g., Saltzman and Edwards, 2017 and references therein). Additionally, the 'biological pump' maintains vertical $\delta^{13}C$ seawater gradients, which are then imprinted on the local carbonates during precipitation. It is unlikely, however, that vertical seawater $\delta^{13}C$ gradients had much of an impact on the strata from our study sites, as they were deposited in an ancient epeiric sea and continental margin settings.

Covariations in $\delta^{13}C$ and $\delta^{34}S$ from multiple sections have been interpreted as recording changes in global oceanic redox conditions (e.g., Gill et al., 2007; Owens et al., 2013). A global expansion of reducing conditions (e.g., euxinia) can lead to enhanced burial rates of organic carbon and pyrite, which will ultimately lead to more positive seawater $\delta^{13}C$ and $\delta^{34}S_{CAS}$ values and be recorded in the geochemistry of marine carbonates. Additionally, $\delta^{34}S_{pyr}$ records have the potential to constrain local redox conditions, and the isotopic difference ($\Delta^{34}S$) between marine sulfate (i.e., $\delta^{34}S_{CAS}$) and sedimentary pyrite compositions which can provide additional environmental information. Relative changes in seawater sulfate concentrations can be inferred from $\Delta^{34}S$, which help to provide independent constraints on the extent of oceanic anoxia and pyrite burial during global carbon cycle perturbations (e.g., Gill et al., 2011).

2.3. I/Ca as a local carbonate redox proxy

Unlike the previously discussed global proxies, local proxies can illuminate various paleoenvironmental conditions for geographically widespread localities that represent an equivalent time interval. Iodine to calcium ratios (I/Ca) measured from carbonate rocks have been recently developed as a novel proxy for local upper-ocean redox conditions (Lu et al., 2010, 2016; Hardisty et al., 2014, 2017; Owens et al., 2017). Iodine is highly sensitive to free oxygen conditions, and under a well-oxygenated water column it occurs as iodate (IO_3^-) (Lu et al., 2010). Iodate concentrations decrease in tandem with decreasing dissolved oxygen, and under sub-oxic to anoxic (including but not limited to euxinia) conditions, when the reduced form, iodide (I^-), becomes dominant (Lu et al., 2016). During carbonate formation IO_3^- is preferentially bound within the carbonate lattice, and therefore iodine concentrations in bulk carbonates can track relative water column oxygenation (Lu et al., 2010). Previous work has documented iodine speciation in the modern oceans (Rue et al., 1997) and I/Ca values of foraminifera tests from variable modern oxygen conditions (Lu et al., 2016), and I/Ca has been applied to paleoceanographic (de)oxygenation events (Hardisty et al., 2017; Lu et al., 2018).

Iodine has a reasonably long residence time in seawater (~300 kyr), which leads to fairly uniform total [I] in modern oceans. However, local oceanographic conditions (e.g. upwelling zones, oxygen minimum zones-OMZs, etc.) can strongly affect the speciation of iodine in the upper ocean (Rue et al., 1997). Iodate reduction to iodide in OMZs leads to marked drops in [IO_3^-] locally in the upper ocean, such that modern planktonic foraminifera record near zero values of I/Ca above shallow OMZs (Lu et al., 2016). In contrast, planktonic forams record much higher I/Ca values of >3 μmol/mol in modern well-oxygenated sites. Further support for this novel proxy can be found in recent I/Ca records from several sites across the Atlantic Ocean basin, documenting various spatial trends in I/Ca during the widely documented Cretaceous Oceanic Anoxic Event 2 (Zhou et al., 2015). Foraminifera-based I/Ca records spanning the Paleocene–Eocene Thermal Maximum also show a range of local redox conditions in both upper water column (planktonic species I/Ca) and bottom waters (benthic species I/Ca) during a global deoxygenation event (Zhou et al., 2014). Thus, I/Ca or I/(Ca+Mg) are novel independent geochemical tools that can evaluate local paleoredox conditions alongside more established proxies for changes in global redox conditions and carbon burial. Magnesium is included to account for dolomitization and the very small amounts of dolomite observed in petrographic examination of samples (Hardisty et al., 2014).

3. Methods

3.1. Sample preparation

Following collection of carbonate samples, we utilized a variety of sample preparation techniques and analyses to ensure that only non-weathered and least altered carbonate components were used for the geochemical analyses outlined below. Carbonate-associated sulfate extractions were carried out on each sample using a similar procedure to that outlined by Wotte et al. (2012). I/(Ca+Mg) analysis was carried out using a similar procedure as described by Lu et al. (2010). More detailed information regarding sample preparation procedures and all geochemical methods can be found in the supplemental methods file of the supplementary material.

3.2. Geochemical analyses

Homogenized $BaSO_4$ and Ag_2S powders were loaded into tin capsules with excess V_2O_5 and analyzed for their $\delta^{34}S$ content by the SO_2-method using a Thermo EA-Isolink coupled to a Thermo Delta V Plus isotope ratio mass spectrometer via a Conflo IV split interface. All isotope ratios are reported in per mil (‰) using delta notation relative to Vienna Canyon Diablo Troilite (V-CDT). Calibration of our samples via the SO_2-method was done based on laboratory standards calibrated relative to the IAEA S-1 standard ($\delta^{34}S$, −0.30‰) and NBS-127 ($\delta^{34}S$, +20.3‰). Analytical reproducibility was better than ±0.2‰ for standards and duplicate samples all of which were analyzed at the National High Magnetic Field Laboratory at Florida State University (NHMFL-FSU). All new $\delta^{13}C$ and $\delta^{18}O$ measurements reported here were done using standard methods for carbonate and bulk organic matter stable isotopic analyses (see appendix for more details on analytical methods) carried out at the NHMFL-FSU.

I/(Ca+Mg) was measured using an Agilent 7500cs inductively-coupled-plasma mass-spectrometer (ICP-MS) at the NHMFL-FSU. Potassium iodate (Fisher Scientific product P253-100) was dissolved, diluted gravimetrically, and mixed with pure elemental standards of Ca^{2+} and Mg^{2+} to make the standard curve to calibrate the samples. The accuracy of this procedure was based on measurements of a known material (KL 1-1; e.g. Hardisty et al., 2014) and was found to be within ±0.5% of the reported

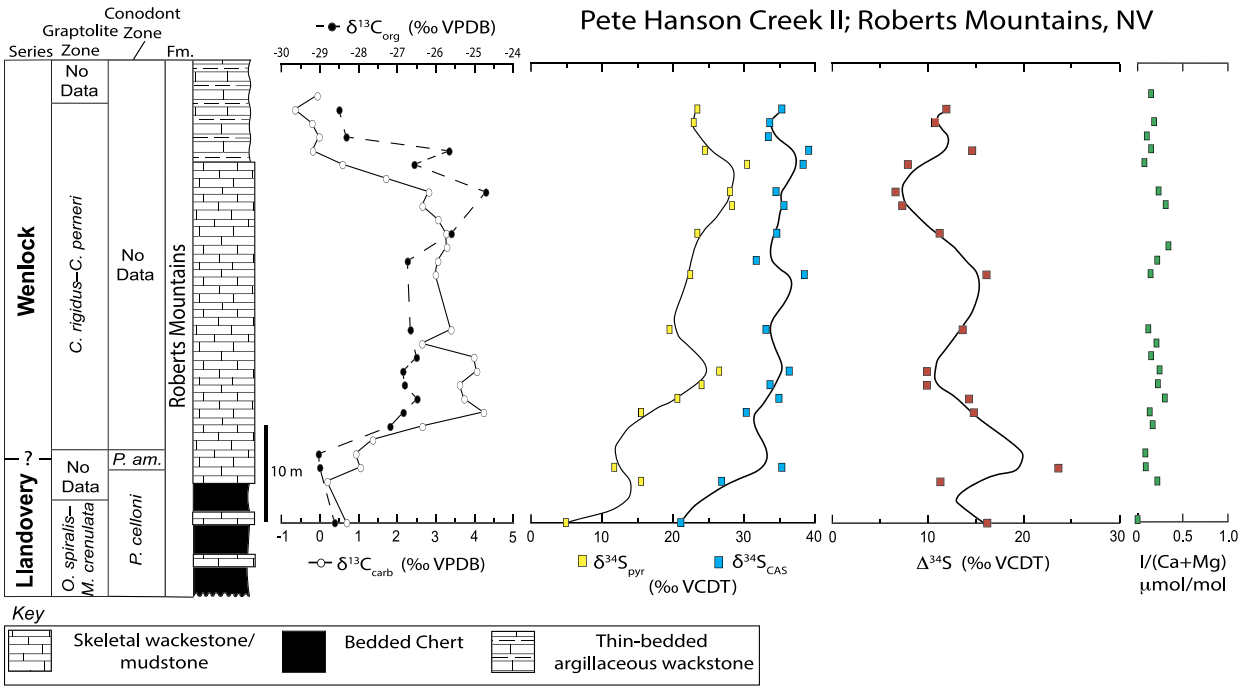

Fig. 2. Geochemical data and lithofacies from the Pete Hanson Creek II section, Roberts Mountains area, NV. Also plotted are conodont and graptolite biozones from previous biostratigraphic studies at the same section (Berry and Murphy, 1975; Klapper and Murphy, 1975).

value. Additionally, precision based on replicate analyses of this same reference material and duplicate samples processed was ±0.08 μmol/mol or better.

4. Results

4.1. Roberts Mountains, Nevada

The thick late Llandovery through Pridoli section exposed near Pete Hanson Creek in the Roberts Mountains has previously been studied for $\delta^{13}C_{carb}$ chemostratigraphy at a coarse sampling resolution (Salzman, 2001). Our new $\delta^{13}C_{carb}$ data captures the entire Ireviken CIE (Fig. 2 and Table S1) within the lower Roberts Mountains Formation, with baseline values recorded near 0‰ and peak positive excursion values of +4.2‰ at 12 m. Additionally, our new $\delta^{13}C_{org}$ values show a positive excursion that covaries with $\delta^{13}C_{carb}$ data, beginning with values at −29.0‰ that shift to peak values of −25.0‰, and then return to baseline values of −28.5‰. The $\delta^{34}S_{CAS}$ data show a positive excursion, with values that begin at +21.1‰ and then shift to values as positive as +39.1‰, which are generally coupled with the $\delta^{13}C$ record. The $\delta^{34}S_{CAS}$ values in the Roberts Mountains Formation remain high as $\delta^{13}C_{carb}$ and $\delta^{13}C_{org}$ records return to baseline values, with $\delta^{34}S_{CAS}$ values only slightly declining to +33.4‰ in the uppermost part of the section. Additionally, $\delta^{34}S_{pyr}$ values shift positively in concert with $\delta^{34}S_{CAS}$ data, from +4.8‰ to as high as +30.4‰. The I/(Ca+Mg) values are consistently very low and show little to no variation throughout this section with values ranging between 0.0 to 0.3 μmol/mol.

4.2. Newsom Roadcut, Tennessee

The $\delta^{13}C_{carb}$ values are replotted (Fig. 3 and Table S2) from Cramer and Saltzman (2005, 2007). These values were not reproduced for this study due to the previously high-sampling-resolution and our stratigraphic sampling being within 10–20 cm of the previous study. It should be noted that this site captures $\delta^{13}C_{carb}$ values that represent the end of the rising limb of the Ireviken CIE to maximum CIE values, as well as the falling-limb to post-excursion $\delta^{13}C_{carb}$ values. The $\delta^{34}S_{CAS}$ data show a pronounced excursion with values starting at +26.3‰ and then values shift back to +18.7‰, which broadly parallels the positive $\delta^{13}C_{carb}$ excursion (i.e. the Ireviken CIE). There is an offset in return to baseline values, however, with $\delta^{13}C_{carb}$ values declining first, followed by $\delta^{34}S_{CAS}$ values that shift several meters later. Following the return in $\delta^{34}S_{CAS}$ values from 6 to 10 m, $\delta^{34}S_{CAS}$ begins to shift back to more positive values, from +22.9‰ to +24.0‰, in the upper 2 m of the section. The I/(Ca+Mg) ratios are at peak values (between 2–2.5 μmol/mol) within the first three meters of the lower Wayne Formation. Then, I/(Ca+Mg) values begin to decrease upsection, to a low (0.1–0.3 μmol/mol) prior to the return to baseline of $\delta^{13}C_{carb}$ and $\delta^{34}S_{CAS}$ values.

4.3. Carbon and sulfur model

For this study, we constructed a forward geochemical box model for $\delta^{13}C$ and $\delta^{34}S$ to illuminate the global burial flux of reduced species required to recreate the observed excursions during the Ireviken Event. Initial boundary conditions and fluxes were prescribed based on modern values (Kurtz et al., 2003), previously published work (Gill et al., 2011; Jones and Fike, 2013), and modified based on our baseline values (Table S3). Individual parameters were perturbed to recreate the observed isotopic trends using Stella® modeling software (similar to Gill et al., 2011; Owens et al., 2013 and references therein). The most plausible explanation of the data is shown in Fig. 4, which uses parameters that best fit with previously published data (e.g., Cramer and Saltzman, 2005) and isotopic data presented in this work. Our ideal model to recreate a +4‰ CIE started with near-modern parameters (Table S3) and perturbed total organic carbon burial to 172% during the event. To recreate an ∼+11‰ excursion in sulfate sulfur isotopes (between the two $\delta^{34}S_{CAS}$ excursion magnitudes) the model started with a 5 mM sulfate reservoir, the pyrite fractionation (offset of final product minus starting composition i.e. $\Delta^{13}C$ and $\Delta^{34}S$) started at −32‰ and was perturbed to −20‰ for the

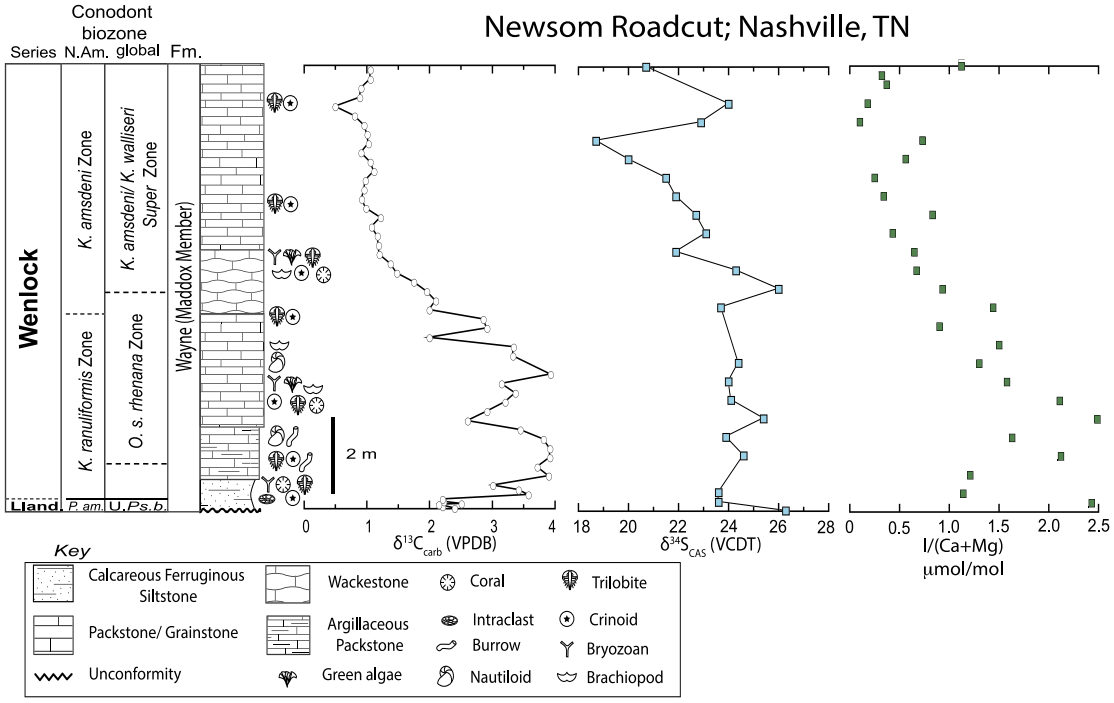

Fig. 3. Geochemical data and lithofacies from Newsom roadcut near Nashville, TN. Also replotted are previous $\delta^{13}C$ data of Cramer and Saltzman (2005, 2007) and conodont biozones from previous work (Barrick, 1983) with new global biozonation scheme incorporated from McAdams et al. (2019).

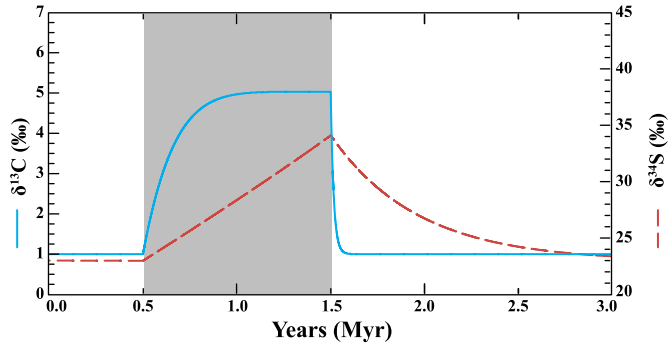

Fig. 4. Modeling of the positive carbon- (solid blue) and sulfur- (dashed red) isotope excursion, with the gray bar indicating the one-million-year (Myr) Ireviken carbon isotope excursion as delineated by the C-isotope profile. In this model the initial marine sulfate concentrations were 5 mM, $\Delta^{34}S$ was decreased during the event to −20‰, pyrite burial increased 339%, and OC burial was increased 172% during the event.

duration of the event (as the data suggest), and the burial of pyrite was increased to 339% for the event.

There are numerous parameter permutations that can recreate the observed isotopic trends, which were individually examined using sensitivity tests for both carbon and sulfur isotopes (Figs. S1 and S2) and reservoir concentrations (Figs. S1 and S2B, D, F, and H). The magnitude of the excursion is controlled by (1) the burial amount of reduced species (Figs. S1A and S2A), (2) the fractionation factor for each isotopic system (Figs. S1E and S2E), and (3) the weathering flux (Figs. S1G and S2G)—the excursion magnitude is not dictated by initial reservoir size (Figs. S1C and S2C), but the response time varies. It should be noted that the DIC pool can be completely exhausted due to increasing organic carbon burial greater than 179% (Fig. S1B), decreasing the initial reservoir size below 3.6×10^{18} mol (Fig. S1D), or by decreasing weathering below 99% (Fig. S1H) of the initial values. Similarly, the sulfate pool can be completely consumed with pyrite burial greater than 401% (Fig. S2B), an initial reservoir size less than 3.5 mM (Fig. S2D), or a weathering flux less than 73% (Fig. S2H) of the initial values. In the ideal model the increased burial of organic carbon and pyrite reduced the reservoir size but did not completely exhaust the marine reservoir of DIC and sulfate (Fig. S2).

5. Discussion

5.1. Diagenetic assessment of geochemical data

Due to the chemical nature of carbonate rocks, diagenesis has the potential to affect the preservation of primary geochemical signatures. Carbonate recrystallization during diagenetic processes can impact $\delta^{13}C_{carb}$, $\delta^{18}O_{carb}$, and $\delta^{34}S_{CAS}$ through fluid interactions and incorporation of lighter isotopes from meteoric waters or pore fluids that may be derived from oxidation of reduced species of carbon or sulfur (sedimentary pyrite), from soil, or from the surrounding rock/sediments. Cross-plots of our $\delta^{13}C_{carb}$ and $\delta^{18}O_{Carb}$ data (Fig. S3A) from Nevada show no signification correlation ($R^2 < 0.1$), while the previous stable isotope data from Tennessee (Cramer and Saltzman, 2005) show a weak to moderate correlation ($R^2 = 0.46$). Cramer and Saltzman (2005) argue the Tennessee trends and variability in the $\delta^{13}C_{carb}$ and $\delta^{18}O_{carb}$ values are mostly primary in nature as they overlap with coeval brachiopod-based $\delta^{13}C_{carb}$ and $\delta^{18}O_{carb}$ stratigraphic trends and values from Gotland, Sweden (Bickert et al., 1997; Munnecke et al., 2003). Diagenesis can also affect primary $\delta^{13}C_{org}$ values due to thermal alteration or respiration of specific organic compounds (e.g., Kump et al., 1999 and references therein). If diagenetic alteration occurred in organic matter-lean versus -enriched horizons we might expect to see systematic trends between $\delta^{13}C_{org}$ and wt.% TOC, but we see no relationship in our data (Fig. S3B). Furthermore, conodont alteration indices from our study sites indicate organic matter experienced low (<100 °C) to moderate alteration temperatures (Klapper and Murphy, 1975; Barrick, 1983).

It has been documented that the concentrations of sulfate and iodate within the carbonate lattice decrease during alteration, as meteoric fluids have lower concentrations than the original calcite (Gill et al., 2008; Hardisty et al., 2017). Therefore, concentrations

of sulfate ([CAS]) and iodate (I/Ca+Mg) should negatively correlate with increased diagenetic alteration, although these diagenetic processes have been shown to have little to no effect on $\delta^{34}S_{CAS}$ values (Gill et al., 2008). Dolomitization of carbonates and precipitation of authigenic dolomites in reducing marine pore fluids tends to lower I/(Ca+Mg) values (Hardisty et al., 2017). It has also been shown, however, that many Paleozoic dolomites can in fact preserve primary seawater I/(Ca+Mg) values if they formed penecontemporaneously with seawater (e.g., Lu et al., 2018). From a combination of petrographic observations and overall low [Mg] during I/(Ca+Mg) analysis, dolomite was found to compose a very minor carbonate component in samples from both of our field localities. Therefore, it's unlikely that decreases in I/(Ca+Mg) values are due to dolomitization of primary fabrics. We observe very weak to no correlation between $\delta^{18}O_{carb}$ vs. $\delta^{34}S_{CAS}$, $\delta^{18}O_{carb}$ vs. [CAS], I/(Ca+Mg) vs. [CAS], and I/(Ca+Mg) vs. $\delta^{34}S_{CAS}$ of our study sites (Fig. S3C–F) suggesting no significant diagenetic overprinting of primary marine I/(Ca+Mg) and $\delta^{34}S_{CAS}$ values.

Sedimentary pyrite oxidation can also impact $\delta^{34}S_{CAS}$ records, as pyrite is a reactive mineral and partial oxidation can occur during later stages of diagenesis or during chemical extraction of CAS if exposed to oxidizing or highly acidic conditions (e.g., Wotte et al., 2012). Incorporation of this oxidized sedimentary pyrite into the dissolved CAS fraction can artificially decrease $\delta^{34}S_{CAS}$ values. Horizons and stratigraphic intervals that had visible pyrite were specifically avoided during sampling. Additionally, all samples extracted for CAS had low sedimentary pyrite content (S_{pyr} < 100 ppm), and cross-plots of [S_{pyr}] vs. $\delta^{34}S_{CAS}$ values show no correlation. Because sedimentary pyrite is typically ^{34}S-depleted relative to seawater sulfate pyrite oxidation cannot be a significant factor influencing the observed stratigraphic trends in $\delta^{34}S_{CAS}$ and $\delta^{34}S_{pyr}$ values, as they document a positive excursion.

Whereas we cannot rule out diagenetic effects entirely, as the secondary minor variations could be attributed to post-burial alteration, by and large diagenesis is not a major factor contributing to the dominant first-order geochemical trends observed. One of the strongest lines of evidence for the preservation of primary geochemical signatures in our data is the consistency of isotopic trends observed at two study sections relative to previous $\delta^{13}C$ records from Baltica and Laurentia that are correlated independently using conodont biostratigraphy (Klapper and Murphy, 1975; Barrick, 1983; Saltzman, 2001; Cramer and Saltzman, 2005, 2007; Cramer et al., 2010).

5.2. Late Llandovery–early Wenlock marine redox conditions

These Tennessee and Nevada sections represent diverse sedimentary environments (shallow inner shelf/epeiric sea versus deeper upper slope) that were connected to the Rheic and Panthalassic ocean basins, respectively. Despite these different depositional environments, the similarities among the geochemical trends indicate their global and dominantly primary nature. Further support for the global nature of these trends is found in a recent study from Gotland, Sweden (paleocontinent of Baltica) that documents a parallel CIE and a +7 to +10‰ excursion in $\delta^{34}S_{CAS}$ that coincides with the Ireviken Event (Rose et al., 2019). The paired positive $\delta^{13}C$ and $\delta^{34}S$ excursions are now documented from three widely separated basins that span the Llandovery/Wenlock boundary, suggesting that the Ireviken CIE records transient increases in organic carbon and pyrite burial under expanded reducing conditions in the global oceans at this time. The parallel behavior between our $\delta^{13}C$ and $\delta^{34}S$ records is consistent with other positive $\delta^{13}C$ and $\delta^{34}S$ excursions in the Phanerozoic record, used widely as proxy evidence for global pyrite burial, suggesting expanded euxinic conditions during short-term perturbations (Gill et al., 2011; Owens et al., 2013; Sim et al., 2015; Edwards et al., 2018). The $\delta^{34}S_{CAS}$ records at both Tennessee and Nevada record a +8‰ and +18‰ magnitude excursion, respectively. These isotopic differences suggest that the sulfate reservoir in the early Silurian oceans was spatially heterogeneous and concentrations significantly lower than the modern ocean (Gill et al., 2007; Lowenstein et al., 2003), which is also observed for other Phanerozoic events. An interesting relationship is observed in our $\delta^{13}C_{carb}$ and $\delta^{34}S_{CAS}$ records at both field sites, where $\delta^{34}S_{CAS}$ remain heavy as $\delta^{13}C_{carb}$ returns to baseline values at the end of the Ireviken CIE. This suggests that elevated rates of pyrite burial persisted, even after the burial of organic matter had slowed. This temporal offset between $\delta^{34}S$ and $\delta^{13}C$ has also been documented in the Early Ordovician (Tremadocian; Edwards et al., 2018) and Cretaceous OAE 2 (Owens et al., 2013). At the Nevada section, $\delta^{34}S_{pyr}$ values shift positively in concert with $\delta^{34}S_{CAS}$ record, with a relatively small $\Delta^{34}S$ that decreases slightly through the excursion from ~15–20‰ to ~6–12‰. It is unlikely that this shift in $\delta^{34}S_{pyr}$ was due to changes in local redox as independent proxy evidence suggest dissolved O_2 was very low throughout the sequence (see I/Ca+Mg discussion below). This parallel excursion in CAS and sedimentary pyrite isotope records supports a primary global pyrite burial signature from pyrite that formed in an open-system near the sediment-water interface, with a locally reducing water-column nearby. Synchronous positive excursions in Llandovery/Wenlock boundary $\delta^{34}S_{pyr}$ and $\delta^{34}S_{CAS}$ records are also documented from Gotland, Sweden (Rose et al., 2019). While there are small offsets in magnitude and baseline values that are likely related to local depositional environments, this provides additional support for a decrease in marine sulfate concentrations linked to global pyrite burial increases.

Evidence for local anoxia (independent of sulfide) is interpreted using I/(Ca+Mg) values from both Nevada and Tennessee, that document very low values and suggest locally reducing water columns. The I/(Ca+Mg) dataset for Nevada (Fig. 2) shows low values (<0.5 μmol/mol) throughout, suggesting a redox-stratified water column near this deeper-water setting before, during, and after the Ireviken CIE. The I/(Ca+Mg) values from Nevada are very similar to I/Ca values found in planktonic carbonates that were deposited very near modern-day oxygen minimum zones (Lu et al., 2010, 2016; Hoogakker et al., 2018). Similar ranges of I/Ca values have been observed during times of transitional oxygenation of marine environments, where anoxic deep waters were likely prevalent and potentially expanded into upwelling zones. Specifically, low I/Ca values have been observed through an Early Ordovician extinction event recorded from deeper-water carbonates in Nevada (Edwards et al., 2018). This has also been documented in the Paleoproterozoic (Hardisty et al., 2014), and across the Permian/Triassic boundary and associated major mass extinction (Loope et al., 2013). I/Ca values with comparable ranges have also been observed during the Cretaceous OAE 2 (e.g., Owens et al., 2017) and from the Eastern Tropical Pacific OMZ during the last glacial maximum (Hoogakker et al., 2018). The low I/(Ca+Mg) values reported here are consistent with previous interpretations of depositional environment and paleoceanographic setting for the Roberts Mountains Formation (Johnson and Murphy, 1984; Cramer and Saltzman, 2005, 2007) and with the $\delta^{34}S_{pyr}$ values (discussed above) that suggest a locally redox-stratified water column.

The I/(Ca+Mg) values in Tennessee are also low overall, although they begin relatively high (2.5–1.2 μmol/mol) indicating a more oxic water column locally during the rising limb to initial peak values of the Ireviken CIE and the initial transgression in sea level. However, I/(Ca+Mg) values do decrease in concert with a continued rise in sea level, suggesting the water column became more reducing and was influenced by greater redox stratification after the Ireviken CIE in Tennessee. Carbonate facies in Tennessee are fossiliferous throughout the section suggesting oxy-

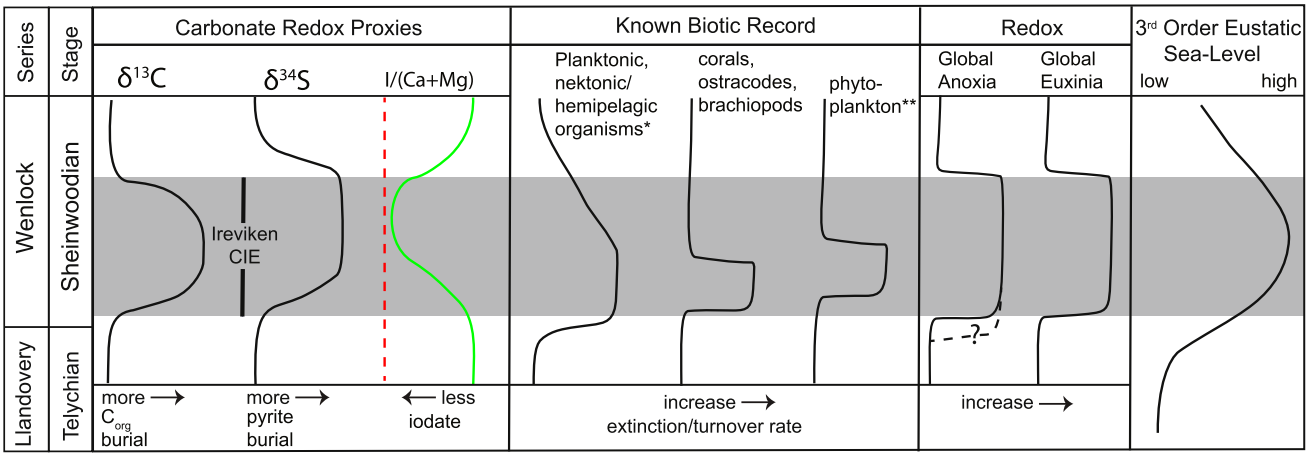

Fig. 5. Generalized stratigraphic changes of carbon and sulfur isotopes ($\delta^{13}C_{carb}$ from Cramer et al., 2010; $\delta^{34}S_{CAS}$ from this study) and I/(Ca+Mg) ratios (this study: red, Nevada and green, Tennessee), redox conditions (from this study), and biotic turnover/extinction rates (Jeppsson, 1997; Melchin et al., 1998; Munnecke et al., 2003; Calner, 2008; Cooper et al., 2014) during the Ireviken CIE. *Note that this curve represents the generalized extinction patterns for conodonts and graptolites relative to $\delta^{13}C_{carb}$ (e.g., Cramer et al., 2010). **Note that this generalized curve represents acritarch (organic-walled phytoplankton) extinctions of which the majority occurred notably after the other marine extinctions took place (e.g., Calner, 2008). The 3rd order eustatic sea-level curve is modified from Cramer and Saltzman (2007).

genated surface conditions prevailed, and there are no apparent diagenetic differences in the low versus high I/(Ca+Mg) intervals of this shallow-water section. These low I/(Ca+Mg) values after the Ireviken CIE suggest an expansion of local anoxia near the western Tennessee Shelf after the global signature, potentially due to local/regional restriction and subsequent shallowing of the oxycline within the Reelfoot Rift embayment during eustatic sea level fall (e.g., Cramer and Saltzman, 2005). The predominantly low I/(Ca+Mg) values presented here are consistent with a recent I/Ca compilation throughout Earth history, that point to a widespread shallow oxycline in Paleozoic oceans underlying oxygenated surface oceans (Lu et al., 2018). Furthermore, the trend in I/(Ca+Mg) values we document from Tennessee are of similar magnitude to previous studies that have indicated local redox shifts within records of low overall I/Ca values (e.g., Proterozoic, Early Ordovician, and Cretaceous OAE 2; Hardisty et al., 2014, 2017; Owens et al., 2017; Edwards et al., 2018).

5.3. Modeling Silurian carbon and sulfur cycles

Conodont and graptolite biozones, along with new radiometric ages, constrain the duration of the Ireviken CIE and the anoxic (likely euxinic) event to approximately one million years, with <500 kyr duration for each individual biozone that spans this interval (Cramer et al., 2010). Thus, the modeling uses a perturbation of one million years for the duration, but the exact duration does not alter the first-order observations. The forward geochemical box model provides quantitative constraints on unknown variables of the C- and S-isotope systems. Our modeling suggests that the C- and S-isotope excursions require a substantial amount of organic carbon and pyrite burial to drive the observed excursions. The amount of organic carbon burial is similar to model estimates for Mesozoic oceanic anoxic events (Kump and Arthur, 1999; Owens et al., 2018) that use near-modern background fluxes. However, if the starting fluxes were much greater, then the organic carbon burial would need to be substantially greater (Owens et al., 2018).

The magnitude of the global S-isotope excursion has been used to quantify the global pyrite burial, which is similar to other studies that have estimated the maximum global extent of seafloor euxinia for other Phanerozoic events at ~5 to 10% (Gill et al., 2011; Owens et al., 2013). Importantly, additional trace metal proxies from shales have similar estimates (Gill et al., 2011: Owens et al., 2016; Dickson, 2017). The assumption that all the increased pyrite burial was entirely deposited under euxinic conditions is likely an oversimplification (Gill et al., 2011; Owens et al., 2013), as other redox environments could also experience enhanced pyrite burial. This estimate represents a maximum, but could be less widespread if there is significant pyrite burial under other redox conditions. However, this assumption is reasonable given that the modern ocean has a disproportionate burial flux to seafloor area (~0.15%) for pyrite in euxinic settings. Additionally, organic sulfur can be an important factor, but quantities and isotopic values are unknown for this event and would have been incorporated into the pyrite burial flux for this model if available (Owens et al., 2013). The estimated total amount of pyrite burial required (339% increase) to recreate a $\delta^{34}S$ excursion of +11‰ (Fig. 4) is ~1.7×10^{18} mol of sulfur, and the sensitivity tests range from ~1.4 to 2.1×10^{18}. Utilizing calculations from Owens et al. (2013), this equates to a maximum extent of ~8.2% of euxinic seafloor area during the Ireviken CIE. This assumes that mass accumulation rates and Fe availability during this event were similar to modern euxinic environments. Whereas this is a substantial increase in reducing environments, which likely increased in the water column above highly productive continental margins, this does not imply that the entire ocean was euxinic or even reducing. This work provides the first global quantitative estimates for redox conditions during the Ireviken Event, and suggests this could have been the dominant driver of the geochemical and biological perturbations during this time.

5.4. Biotic response (Ireviken Event) to widespread anoxia

Global biotic records across the Llandovery/Wenlock boundary document a major marine extinction event in the early Silurian oceans (e.g., Talent et al., 1993; Jeppsson, 1997; Melchin et al., 1998; Calner, 2008). There was an extinction of ~80% of the known global conodont species, known as the 'Ireviken Event' after the type-locality preserved on Gotland, Sweden (Jeppsson, 1997). Conodont faunas show a stepwise extinction, up to 10 separate 'datum points' (extinction steps), that can be subdivided into as many as 8 conodont biozones (e.g., Cramer et al., 2010). Additionally, there was a major extinction in graptolites (Melchin et al., 1998), where global species richness dropped sharply by ~50%, and this extinction intensity matches the Hirnantian Stage and corresponding Late Ordovician Mass Extinction (Crampton et al., 2016). Trilobites also experienced major declines during this time interval, with ~50% of species becoming extinct (e.g., Calner, 2008). Records

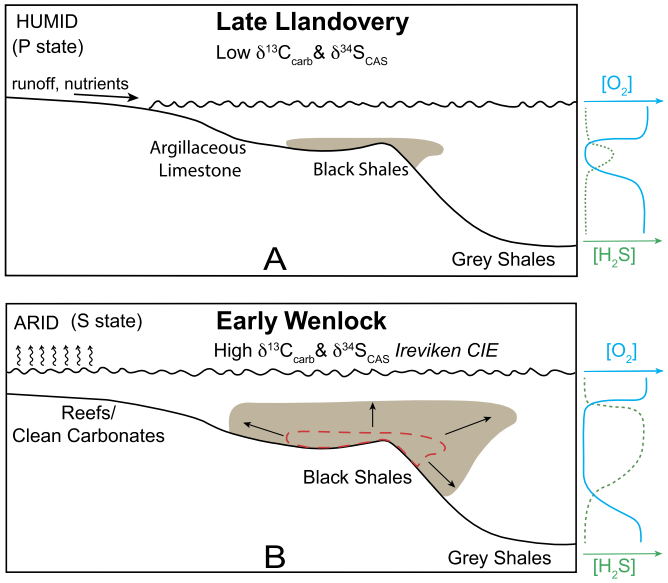

Fig. 6. Schematic reconstruction of redox evolution across the Llandovery–Wenlock boundary in the early Silurian. A, Late Llandovery paleoceanographic reconstruction showing relatively small area of water-column/sea floor anoxic/euxinic conditions that produce black shales in distal shelf settings during initial transgression (modified after Cramer and Saltzman, 2007). B, Early Wenlock paleoceanographic reconstruction showing an expansion of stratified reducing conditions (anoxic/euxinic) further into shelf/slope settings during sea level high stand. Insets to the right show average profiles for dissolved O_2 and H_2S, please note the expanded area of deoxygenated seafloor and water-column conditions during the early Wenlock that coincides with positive excursions in $\delta^{13}C_{carb}$ and $\delta^{34}S_{CAS}$ and rise in sea level.

of acritarchs (a major Paleozoic phytoplankton group), chitinozoans, corals, and brachiopods all show major taxonomic declines and increases in extinction rates (e.g., Munnecke et al., 2003; Calner, 2008). These biotic records have been very well integrated with $\delta^{13}C_{carb}$ records specifically in successions from Baltica and Laurentia. Specifically, the onset of the Ireviken CIE has been correlated with Datums 2 to 4 of the Ireviken Event, and not only are conodont taxa declining but graptolite and trilobite extinction events correspond to this specific interval (Calner, 2008; Cramer et al., 2010). These observations combined with our new geochemical data indicate that these marine taxa were most likely affected by the same event that caused the perturbations to the global carbon and sulfur cycles. Thus, a major biogeochemical perturbation during this interval occurred and was likely caused by climatic feedbacks.

It is clear from Silurian biotic records that a significant crisis occurred across the Llandovery/Wenlock boundary interval coincident with $\delta^{13}C$ and $\delta^{34}S$ evidence (Fig. 5) for increased euxinia and likely an expansion of non-sulfidic anoxia. The new I/(Ca+Mg) records show evidence for persistent low-oxygen conditions in outer shelf/upper slope settings of western Laurentia. Whereas, I/(Ca+Mg) records from shallow shelf/epeiric sea settings in southern Laurentia indicate initially oxygenated conditions that then became impacted by O_2-depleted waters during the later stages of the Ireviken CIE. Marine taxa from a wide range of ecological niches, including pelagic planktonic graptolites to sessile epifaunal corals and brachiopods, were affected by this extinction event. Nektonic/nektobenthic conodonts, pelagic zooplanktonic graptolites, and pelagic/nektobenthic trilobites were clearly the most strongly affected marine groups during this extinctions event, while reef organisms, brachiopods, and ostracodes were impacted to a lesser extent (Munnecke et al., 2003). Detailed biotic records through this interval reveal that conodonts, graptolites, and trilobite extinctions/turnovers began first, followed later by corals, ostracodes, and brachiopods, and turnovers in acritarchs (Calner, 2008). This pattern of extinction coincides broadly with sea-level rise across the Llandovery/Wenlock boundary and is consistent with the global expansion of euxinic and local anoxic waters from deeper marine settings into shallower shelf environments (Fig. 6) as a causal mechanism. Carbonate redox proxies (positive $\delta^{34}S_{CAS}$ and low I/[Ca+Mg]) suggest expansion of local anoxia and global euxinia in the extinction interval. Specifically, I/(Ca+Mg) values in Nevada demonstrate that local anoxic water masses predate the extinction, and remain during and after the CIE. Marine biodiversity levels recover during the falling-limb and upon establishment of post-Ireviken CIE baseline $\delta^{13}C$ values (e.g., Cooper et al., 2014), suggesting a trend towards less reducing conditions globally. When combining sequence stratigraphic evidence of sea-level rise with biotic extinction records and new diverse geochemical evidence for perturbed marine redox conditions, this reinforces the view that euxinia was the driver for the Llandovery/Wenlock boundary mass extinction event.

6. Conclusions

The documented stratigraphic trends in geochemical data from Roberts Mountains, Nevada, and Newsom Roadcut, Tennessee highlight the global and local redox conditions before, during, and after the Ireviken CIE and associated extinction event. The $\delta^{34}S_{CAS}$ records show parallel positive behavior with Ireviken $\delta^{13}C_{carb}$ records indicating increased burial of organic carbon and pyrite under widespread euxinic conditions. Furthermore, an offset in post-Ireviken CIE $\delta^{34}S_{CAS}$ and $\delta^{13}C_{carb}$ records suggests burial of pyrite persisted well after organic matter burial declined, similar to paired records from Cretaceous Oceanic Anoxic Event 2 (Owens et al., 2013). The near zero I/(Ca+Mg) values throughout the Roberts Mountains section indicate an oxic surface ocean overlying proximal anoxic water mass with a persistently shallow chemocline. While the I/(Ca+Mg) values from Newsom Roadcut indicate relatively oxic conditions initially in this shallow shelf area that became increasingly exposed to laterally and vertically adjacent anoxic waters during the waning phases of the Ireviken CIE as water masses became possibly restricted and stratified during sea-level fall. These new carbonate multiproxy data assess both local and global paleoredox conditions and reveal strong evidence for local water column anoxia and global increases in seafloor extent of euxinia beginning during the late Llandovery and continuing through early Wenlock. Our datasets presented here are consistent with previous oceanographic and global carbon cycle models invoking increases in organic carbon burial under anoxic conditions (Cramer and Saltzman, 2005, 2007).

We find no geochemical or box model evidence, however, to support a globally anoxic or predominantly stratified deep ocean as previous models have suggested (Bickert et al., 1997; Cramer and Saltzman, 2007). Rather, our data suggest that ~8.2% of the global seafloor area were overlain by euxinic waters during the Ireviken CIE in the early Wenlock, and that these reducing marine waters were most likely situated along continental margins instead of deep-ocean settings (e.g., Lyons et al., 2014). These geochemical data, when placed within the context of pronounced declines in early Silurian marine biota and eustatic sea-level rise, provide consistent evidence for the hypothesis that shoaling of toxic euxinic waters into shelf areas led to the mass extinction event, the Ireviken Event, across the Llandovery/Wenlock boundary. This mechanism and similar supporting geochemical evidence have been documented for other Paleozoic extinction events linked to euxinia including the late Cambrian SPICE event (Gill et al., 2011), Early Ordovician base-Stairsian event (Saltzman et al., 2015; Edwards et al., 2018), Late Devonian *punctata* and Kellwasser events (e.g., Sim et al., 2015), and end-Permian major mass extinction (Loope et al., 2013). The Ireviken CIE and associated extinc-

tion event likely represents one of several major anoxic-euxinic events in the Silurian as biotic and lithologic evidence suggest this could be a recurrent scenario (Jeppsson, 1998; Calner, 2008; Crampton et al., 2016). In broader terms, our study supports recent findings of continued oxygen depletion in subsurface waters of Paleozoic oceans (Sperling et al., 2015; Lu et al., 2018), and that oxygen levels were a major factor in the evolution of Paleozoic biosphere (e.g., Edwards et al., 2017).

Acknowledgements

Erik Sperling and two anonymous reviewers are thanked for their constructive reviews that improved this paper and Derek Vance for editorial direction. Additionally, we thank Theodore Them II for additional comments that improved an earlier draft of this paper. AK would like to thank the Young Lab Group at FSU for their support and assistance in sample collection and geochemical analyses: Chelsie Bowman, Nevin Kozik, and Emily Benayoun. AK would also like to thank Burt Wolff at the National High Magnetic Field Laboratory (NHMFL) for his technical support with the carbon isotope analysis and Benjamin Underwood at Indiana University for his initial help with preliminary sulfur isotope analysis for this project. Funding from NSF (EAR-1748635) to SAY and JDO supported this work, as well as a graduate student research grant from the Geological Society of America to AK. This work was performed at the National High Magnetic Field Laboratory, which is supported by the National Science Foundation Cooperative Agreement No. DMR-1157490 and the State of Florida.

Appendix A. Supplementary material

Supplementary material related to this article can be found online at https://doi.org/10.1016/j.epsl.2019.02.023.

References

Adams, D.D., Hurtgen, M.T., Sageman, B.B., 2010. Volcanic triggering of a biogeochemical cascade during Oceanic Anoxic Event 2. Nat. Geosci. 3, 201–204.

Barrick, J.E., 1983. Wenlockian (Silurian) conodont biostratigraphy, biofacies, and carbonate lithofacies, Wayne Formation, central Tennessee. J. Paleontol. 57, 208–239.

Berner, R.A., VandenBrooks, J.M., Ward, P.D., 2007. Evolution – oxygen and evolution. Science 316, 557–558.

Berry, W.B.N., Murphy, M.A., 1975. Silurian and Devonian graptolites of central Nevada. Univ. Calif. Publ. Geol. Sci. 110, 109.

Bickert, T., Patzold, J., Samtleben, C., Munnecke, A., 1997. Paleoenvironmental changes in the Silurian indicated by stable isotopes in brachiopod shells from Gotland, Sweden. Geochim. Cosmochim. Acta 61, 2717–2730.

Calner, M., 2008. Silurian global events—at the tipping point of climate change. In: Ashraf, M.T. (Ed.), Mass Extinctions. Springer-Verlag, Berlin, Heidelberg, pp. 21–58.

Canfield, D.E., Raiswell, R., Bottrell, S., 1992. The reactivity of sedimentary iron minerals toward sulfide. Am. J. Sci. 292, 659–683.

Cooper, R.A., Sadler, P.M., Munnecke, A., Crampton, J.S., 2014. Graptoloid evolutionary rates track Ordovician–Silurian global climate change. Geol. Mag. 151, 349–364.

Cramer, B.D., Loydell, D.K., Samtleben, C., Munnecke, A., Kaljo, D., Mannik, P., Martma, T., Jeppsson, L., Kleffner, M.A., Barrick, J.E., Johnson, C.A., Emsbo, P., Joachimski, M.M., Bickert, T., Saltzman, M.R., 2010. Testing the limits of Paleozoic chronostratigraphic correlation via high-resolution (<500 k.y.) integrated conodont, graptolite, and carbon isotope (delta C-13(carb)) biochemostratigraphy across the Llandovery–Wenlock (Silurian) boundary: is a unified Phanerozoic time scale achievable? Geol. Soc. Am. Bull. 122, 1700–1716.

Cramer, B.D., Saltzman, M.R., 2005. Sequestration of C-12 in the deep ocean during the early Wenlock (Silurian) positive carbon isotope excursion. Palaeogeogr. Palaeoclimatol. Palaeoecol. 219, 333–349.

Cramer, B.D., Saltzman, M.R., 2007. Fluctuations in epeiric sea carbonate production during Silurian positive carbon isotope excursions: a review of proposed paleoceanographic models. Palaeogeogr. Palaeoclimatol. Palaeoecol. 245, 37–45.

Crampton, J.S., Cooper, R.A., Sadler, P.M., Foote, M., 2016. Greenhouse-icehouse transition in the Late Ordovician marks a step change in extinction regime in the marine plankton. Proc. Natl. Acad. Sci. USA 113, 1498–1503.

Dickson, A.J., 2017. A molybdenum-isotope perspective on Phanerozoic deoxygenation events. Nat. Geosci. 10, 721–726.

Edwards, C.T., Fike, D.A., Saltzman, M.R., Lu, W.Y., Lu, Z.L., 2018. Evidence for local and global redox conditions at an Early Ordovician (Tremadocian) mass extinction. Earth Planet. Sci. Lett. 481, 125–135.

Edwards, C.T., Saltzman, M.R., Royer, D.L., Fike, D.A., 2017. Oxygenation as a driver of the Great Ordovician Biodiversification Event. Nat. Geosci. 10, 925.

Fry, B., Jannasch, H.W., Molyneaux, S.J., Wirsen, C.O., Muramoto, J.A., King, S., 1991. Stable isotope studies of the carbon, nitrogen and sulfur cycles in the Black-Sea and the Cariaco Trench. Deep-Sea Res., A, Oceanogr. Res. Pap. 38, S1003–S1019.

Gill, B.C., Lyons, T.W., Frank, T.D., 2008. Behavior of carbonate-associated sulfate during meteoric diagenesis and implications for the sulfur isotope paleoproxy. Geochim. Cosmochim. Acta 72, 4699–4711.

Gill, B.C., Lyons, T.W., Saltzman, M.R., 2007. Parallel, high-resolution carbon and sulfur isotope records of the evolving Paleozoic marine sulfur reservoir. Palaeogeogr. Palaeoclimatol. Palaeoecol. 256, 156–173.

Gill, B.C., Lyons, T.W., Young, S.A., Kump, L.R., Knoll, A.H., Saltzman, M.R., 2011. Geochemical evidence for widespread euxinia in the Later Cambrian ocean. Nature 469, 80–83.

Hardisty, D.S., Lu, Z., Bekker, A., Diamond, C.W., Gill, B.C., Jiang, G., Kah, L.C., Knoll, A.H., Loyd, S.J., Osburn, M.R., Planavsky, N.J., Wang, C., Zhou, X., Lyons, T.W., 2017. Perspectives on Proterozoic surface ocean redox from iodine contents in ancient and recent carbonate. Earth Planet. Sci. Lett. 463, 159–170.

Hardisty, D.S., Lu, Z.L., Planavsky, N.J., Bekker, A., Philippot, P., Zhou, X.L., Lyons, T.W., 2014. An iodine record of Paleoproterozoic surface ocean oxygenation. Geology 42, 619–622.

Hoogakker, B.A.A., Lu, Z.L., Umling, N., Jones, L., Zhou, X.L., Rickaby, R.E.M., Thunell, R., Cartapanis, O., Galbraith, E., 2018. Glacial expansion of oxygen-depleted seawater in the eastern tropical Pacific. Nature 562, 410–413.

Jeppsson, L., 1997. The anatomy of the Mid–Early Silurian Ireviken event and a scenario for P-S events. In: Brett, C.E., Baird, G.C. (Eds.), Paleontological Events: Stratigraphic, Ecological and Evolutionary Implications, pp. 451–492.

Jeppsson, L., 1998. Silurian oceanic events: summary of general characteristics. In: Landing, E., Johnson, M.E. (Eds.), Silurian Cycles: Linkages of Dynamic Stratigraphy with Atmospheric, Oceanic and Tectonic Changes. In: New York State Museum Bull., vol. 491, pp. 239–257.

Johnson, J.G., Murphy, M.A., 1984. Time-rock model for Siluro-Devonian continental shelf, western United States. Geol. Soc. Am. Bull. 95, 1349–1359.

Jones, D.S., Fike, D.A., 2013. Dynamic sulfur and carbon cycling through the end-Ordovician extinction revealed by paired sulfate-pyrite delta S-34. Earth Planet. Sci. Lett. 363, 144–155.

Klapper, G., Murphy, M.A., 1975. Silurian–Lower Devonian conodont sequence in the Roberts Mountains Formation of central Nevada. Univ. Calif. Publ. Geol. Sci. 111, 62.

Kump, L.R., Arthur, M.A., 1999. Interpreting carbon-isotope excursions: carbonates and organic matter. Chem. Geol. 161, 181–198.

Kump, L.R., Arthur, M.A., Patzkowsky, M.E., Gibbs, M.T., Pinkus, D.S., Sheehan, P.M., 1999. A weathering hypothesis for glaciation at high atmospheric $pCO(2)$ during the Late Ordovician. Palaeogeogr. Palaeoclimatol. Palaeoecol. 152, 173–187.

Kurtz, A.C., Kump, L.R., Arthur, M.A., Zachos, J.C., Paytan, A., 2003. Early Cenozoic decoupling of the global carbon and sulfur cycles. Paleoceanography 18.

Loope, G.R., Kump, L.R., Arthur, M.A., 2013. Shallow water redox conditions from the Permian–Triassic boundary microbialite: the rare earth element and iodine geochemistry of carbonates from Turkey and South China. Chem. Geol. 351, 195–208.

Lowenstein, T.K., Hardie, L.A., Timofeeff, M.N., Demicco, R.V., 2003. Secular variation in seawater chemistry and the origin of calcium chloride basinal brines. Geology 31, 857–860.

Lu, W., Ridgwell, A., Thomas, E., Hardisty, D.S., Luo, G., Algeo, T.J., Saltzman, M.R., Gill, B.C., Shen, Y., Ling, H.F., Edwards, C.T., Whalen, M.T., Zhou, X., Gutchess, K.M., Jin, L., Rickaby, R.E.M., Jenkyns, H.C., Lyons, T.W., Lenton, T.M., Kump, L.R., Lu, Z., 2018. Late inception of a resiliently oxygenated upper ocean. Science 361, 174–177.

Lu, Z.L., Hoogakker, B.A.A., Hillenbrand, C.D., Zhou, X.L., Thomas, E., Gutchness, K.M., Lu, W.Y., Jones, L., Rickaby, R.E.M., 2016. Oxygen depletion recorded in upper waters of the glacial Southern Ocean. Nat. Commun. 7, 11146.

Lu, Z.L., Jenkyns, H.C., Rickaby, R.E.M., 2010. Iodine to calcium ratios in marine carbonate as a paleo-redox proxy during oceanic anoxic events. Geology 38, 1107–1110.

Lyons, T.W., Reinhard, C.T., Planavsky, N.J., 2014. The rise of oxygen in Earth's early ocean and atmosphere. Nature 506, 307–315.

McAdams, N.E.B., Cramer, B.D., Bancroft, A.M., Melchin, M.J., Devera, J.A., Day, J.E., 2019. Integrated delta C-13(carb), conodont, and graptolite biochemostratigraphy of the Silurian from the Illinois Basin and stratigraphic revision of the Bainbridge Group. Geol. Soc. Am. Bull. 131, 335–352.

Melchin, M.J., Koren, T.N., Storch, P., 1998. Global diversity and survivorship patterns of Silurian graptoloids. In: Landing, E., Johnson, M.E. (Eds.), Silurian Cycles: Linkages of Dynamic Stratigraphy with Atmospheric, Oceanic and Tectonic Changes. In: New York State Museum Bull., vol. 491, pp. 165–181.

Munnecke, A., Samtleben, C., Bickert, T., 2003. The Ireviken event in the lower Silurian of Gotland, Sweden relation to similar Palaeozoic and Proterozoic events. Palaeogeogr. Palaeoclimatol. Palaeoecol. 195, 99–124.

Owens, J.D., Gill, B.C., Jenkyns, H.C., Bates, S.M., Severmann, S., Kuypers, M.M.M., Woodfine, R.G., Lyons, T.W., 2013. Sulfur isotopes track the global extent and dynamics of euxinia during Cretaceous Oceanic Anoxic Event 2. Proc. Natl. Acad. Sci. USA 110, 18407–18412.

Owens, J.D., Lowery, C.M., Lyons, T.W., 2018. Quantifying the missing sink for global organic carbon burial during a Cretaceous oceanic anoxic event. Earth Planet. Sci. Lett. 499, 83–94.

Owens, J.D., Lyons, T.W., Hardisty, D.S., Lowery, C.M., Lu, Z., Lee, B., Jenkyns, H.C., 2017. Patterns of local and global redox variability during the Cenomanian–Turonian Boundary Event (Oceanic Anoxic Event 2) recorded in carbonates and shales from central Italy. Sedimentology 64, 168–185.

Owens, J.D., Reinhard, C.T., Rohrssen, M., Love, G.D., Lyons, T.W., 2016. Empirical links between trace metal cycling and marine microbial ecology during a large perturbation to Earth's carbon cycle. Earth Planet. Sci. Lett. 449, 407–417.

Rose, C.V., Fischer, W.W., Finnegan, S., Fike, D.A., 2019. Records of carbon and sulfur cycling during the Silurian Ireviken Event in Gotland, Sweden. Geochim. Cosmochim. Acta 246, 299–316.

Rue, E.L., Smith, G.J., Cutter, G.A., Bruland, K.W., 1997. The response of trace element redox couples to suboxic conditions in the water column. Deep-Sea Res., Part 1 44, 113–134.

Saltzman, M.R., 2001. Silurian delta C-13 stratigraphy: a view from North America. Geology 29, 671–674.

Saltzman, M.R., 2005. Phosphorus, nitrogen, and the redox evolution of the Paleozoic oceans. Geology 33, 573–576.

Saltzman, M.R., Edwards, C.T., 2017. Gradients in the carbon isotopic composition of Ordovician shallow water carbonates: a potential pitfall in estimates of ancient CO2 and O-2. Earth Planet. Sci. Lett. 464, 46–54.

Saltzman, M.R., Edwards, C.T., Adrain, J.M., Westrop, S.R., 2015. Persistent oceanic anoxia and elevated extinction rates separate the Cambrian and Ordovician radiations. Geology 43, 807–810.

Sim, M.S., Ono, S.H., Hurtgen, M.T., 2015. Sulfur isotope evidence for low and fluctuating sulfate levels in the Late Devonian ocean and the potential link with the mass extinction event. Earth Planet. Sci. Lett. 419, 52–62.

Sperling, E.A., Wolock, C.J., Morgan, A.S., Gill, B.C., Kunzmann, M., Halverson, G.P., Macdonald, F.A., Knoll, A.H., Johnston, D.T., 2015. Statistical analysis of iron geochemical data suggests limited late Proterozoic oxygenation. Nature 523, 451–454.

Talent, J.A., Mawson, R., Andrew, A.S., Hamilton, P.J., Whitford, D.J., 1993. Middle Paleozoic extinction events – faunal and isotopic data. Palaeogeogr. Palaeoclimatol. Palaeoecol. 104, 139–152.

Trotter, J.A., Williams, I.S., Barnes, C.R., Mannik, P., Simpson, A., 2016. New conodont delta O-18 records of Silurian climate change: implications for environmental and biological events. Palaeogeogr. Palaeoclimatol. Palaeoecol. 443, 34–48.

Vaquer-Sunyer, R., Duarte, C.M., 2010. Sulfide exposure accelerates hypoxia-driven mortality. Limnol. Oceanogr. 55, 1075–1082.

Wotte, T., Shields-Zhou, G.A., Strauss, H., 2012. Carbonate-associated sulfate: experimental comparisons of common extraction methods and recommendations toward a standard analytical protocol. Chem. Geol. 326, 132–144.

Young, S.A., Gill, B.C., Edwards, C.T., Saltzman, M.R., Leslie, S.A., 2016. Middle–Late Ordovician (Darriwilian–Sandbian) decoupling of global sulfur and carbon cycles: isotopic evidence from eastern and southern Laurentia. Palaeogeogr. Palaeocl. 458, 118–132.

Zhou, X.L., Jenkyns, H.C., Owens, J.D., Junium, C.K., Zheng, X.Y., Sageman, B.B., Hardisty, D.S., Lyons, T.W., Ridgwell, A., Lu, Z.L., 2015. Upper ocean oxygenation dynamics from I/Ca ratios during the Cenomanian–Turonian OAE 2. Paleoceanography 30, 510–526.

Zhou, X.L., Thomas, E., Rickaby, R.E.M., Winguth, A.M.E., Lu, Z.L., 2014. I/Ca evidence for upper ocean deoxygenation during the PETM. Paleoceanography 29, 964–975.